Journal of Applied Science and Technology (JAST), Vol. 21, Nos. 1 & 2, 2016, pp. 34 - 41

THERMAL AGEING ANALYSIS AND LIFETIME PREDICTION OF IGBT INVERTER FOR SOLAR PV-GRID ELECTRICITY CONNECTIVITY

R.G. Agbokpanzo, T.K. Houngan, F.X. Fifatin, M. Saleh† and C. Espanet‡
University of Abomey-Calavi, 01BP 2009 Cotonou, Benin
†Catholic University of West Africa, 04BP 928 Cotonou, Benin
‡University of Franche Comte, Parc Technologique, 2 Av. Jean Moulin, 90000 Belfort, France

ABSTRACT

Thermal factors contributing to the ageing of Insulated Gate Bipolar Transistor (IGBT) inverters were investigated, with special reference to temperature variation as the main source of degradation of the electrical insulations and material layers. The inverter configuration was analysed in order to predict the lifetime based on thermal ageing. Therefore, a lifetime prediction model based on NSGA-II algorithm was implemented to identify optimal design condition as a compromise between the average temperature and total mass of the inverter. The option of either choosing design configuration according to using the device during the entire lifetime or half of the lifetime of the solar panel was the major decision. The research findings would contribute to better adaptation of IGBT inverter-solar panel for grid electricity connectivity in relation to the replacement of the invertor once over the lifetime of the panel.

Keywords: *IGBT inverter, solar PV-Grid electricity, NSGA-II algorithm, Thermal ageing, Lifetime prediction*

1. INTRODUCTION

To obtain alternating voltage from direct voltage produced by a solar panel requires three phase inverter, consisting of Insulated Gate Bipolar Transistor (IGBT) module and diode chips. The IGBT modules are complex in design, but are made of different materials which provide good mechanical stability, electrical insulation and thermal conductivity [1].

IGBT inverters connected to PV panels fail after operating for a relatively short time and have to be replaced, due to thermal ageing of the different components at high temperatures. Several factors including electrical, mechanical and thermal effects cause the thermal ageing, and the high operating temperatures and large variations induce failure of the device [2]. Photovoltaic inverters operate at 350 - 750 V under continuously varying solar irradiation.

In this paper, an optimal system design analysis to find most efficient configuration of the IGBT inverter for solar PV-Grid electricity connectivity based on thermal ageing of the different material layers is presented. From the average operating temperature of the IGBT chip, a lifetime prediction model was developed considering the inter-relationships between the various design variables.

2. GEOMETRICAL CONFIGURATION OF IGBT MODULE

The IGBT inverter consisted of six (6) IGBT modules shown in Fig. 1, where the power interrupters (S1-S6) are made of IGBT chips and free wheel diodes, V_{cc} is a continuous voltage, 0 is fictive point, and a, b, and c represent three phases of the inverter. Each module is made of both IGBT chips and diode chips [3].

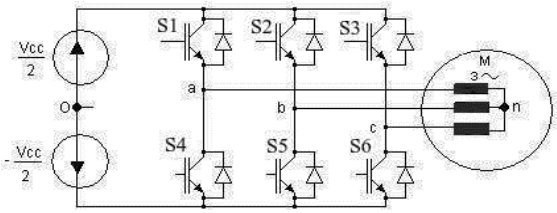

Fig. 1. Electronic circuit of the constructed three phase inverter [4]

Figure 2 shows top view of the inverter arm, where c_i is side of IGBT chip, c_d is side of diode chip, $\ell_{cu,i}$ is width of metallized substrate, $\ell_{br,d}$ is width of solder under diode, $\ell_{br,i}$ is width of solder under IGBT, $L_{br,d}$ is length of solder on the side of diode, $L_{br,I}$ is length of solder on the side of IGBT, ℓ_{sb} is width of the sole and casing, and L_{sem} is length of the sole and casing.

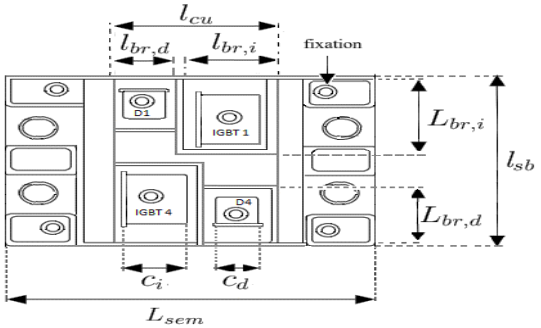

Fig. 2. Top view of an inverter arm [2]

Table 1. Module material properties [1, 7, 8]

Layer Materials	Coefficient of thermal expansion (ppm/°C)	Density (g/cm^3)	Thermal conductivity λ (W/(m K))
Aℓ	22	2.7	237
AℓSiC	8	3	150
AℓN	4	3.26	170
Cu	17	8.96	401
Si	3	2.33	148
Sn(96.5)Ag(3.5)	20.2-22.9	7.30(Sn) 10.5(Ag)	53

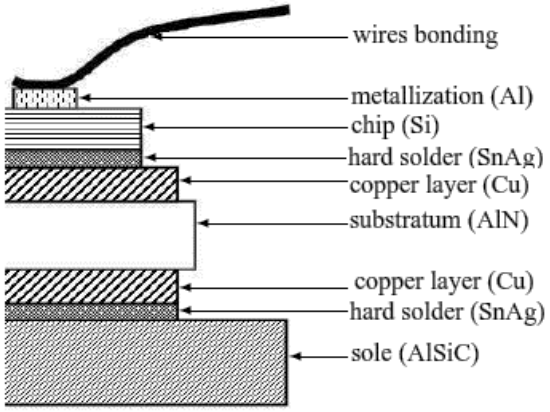

Fig. 3. Different material layers of IGBT module

As shown in Fig. 3, the silicon diode and IGBT chips were soldered on a direct bonded copper (DBC) on each side of aluminum nitride (AℓN) substratum [3]. The AℓN substrate used for the IGBT module investigated offered high thermal conductivity [5, 6]. The substrate was brazed to a sole made of AℓSiC. The solders used were tin-silver alloy (SnAg). The connections between the chips and the copper tracks of the DBC were provided by aluminum bonding wires, i.e. welded ultrasound aluminum wires on aluminum metallization chips.

Figure 3 illustrates the different material layers of IGBT module. The values of coefficient of thermal expansion, density and thermal conductivity of IGBT layer materials are listed in Table 1.

3. THERMAL MODEL OF IGBT MODULE

The characteristics of thermal ageing were examined by analysing a thermal model of the IGBT module to obtain the operational data of the device. The thermal flux generated in the module passed through the semiconductor junctions and the housing before finally being transferred to the ambient environment. Heating of the module was quickly dissipated as the thermal resistivity of the different layers was low.

3.1. Thermal Resistance

By identifying different sections of the module exposed to thermal fluxes, the corresponding thermal circuit adopted for the thermal resistances is shown in Fig. 4 [3], neglecting convective thermal resistance to ambient air. The IGBT module had no external or internal cooling systems, except natural convection via ambient air.

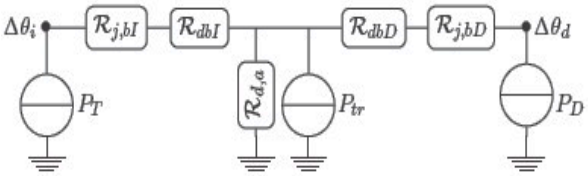

Fig. 4. Thermal resistance model of IGBT inverter 3]

In Fig. 4, $\Delta\theta_i$ and $\Delta\theta_d$ are the respective temperatures at the IGBT and diode junction, such that the average temperature of the inverter was

$$\theta_{avg} = \frac{1}{2}(\Delta\theta_i + \Delta\theta_d) \quad (1)$$

Also P_T is the total losses of IBGT, P_D is total losses of diode, and P_{tr} is parasitic losses of lead resistance (measured in W as power loss).

The thermal resistances (°C/W) of IG BT die and solder ($R_{j,bI}$), diode die and solder ($R_{j,bD}$), case and high solder ($R_{dbI} = R_{dbD}$), and radiator ($R_{d,ar}$), were respectively expressed by the equations [3];

$$R_{j,bI} = \frac{E_{br}}{l_{br,i} l_{br} \lambda_{br}} + \frac{E_{die}}{\lambda_{sil} c_d^2} \quad (2)$$

$$R_{j,bD} = \frac{E_{br}}{l_{br,d} l_{bd} \lambda_{br}} + \frac{E_{die}}{\lambda_{sil} c_d^2} \quad (3)$$

$$R_{dbI} = R_{dbD} = \frac{2E_{cu}}{l_{sb} l_{cu} \lambda_{cu}} + \frac{E_{solder}}{l_{sb} l_{cu} \lambda_{sil}} + \frac{E_{sem}}{l_{sb} L_{sem} \lambda_{AlSiC}} + \frac{E_{sub}}{l_{sb} l_{cu} \lambda_{AiN}} + \frac{E_{cas}}{l_{sb} L_{sb} \lambda_{PBT}} \quad (4)$$

$$R_{d,a} = \frac{E_{radiat}}{l_{sb} L_{sem} \lambda_{radiat}} + \frac{1}{h_{air} l_{sb} L_{sem}} \quad (5)$$

where E_j is thickness of corresponding j layer, and h_{air} is thermal convection coefficient of air.

3.2. Calculation of Thermal Losses

The thermal losses caused by switching

arm of a full bridge inverter formed by IGBT switches and anti-parallel diodes were calculated on the assumptions that the bus voltage was constant, output current of the inverter was sinusoidal, reference voltage was sinusoidal and not phase-shifted, but maintained constant over the switching period [3].

3.2.1. Conduction losses in IGBTs and diodes

Conduction loss in an IGBT module rated as P_{tcond} was obtained by integrating the period of instantaneous power at the terminals. The model was simplified to maximize the losses by using the voltage drop obtained at rated speed of V_{CEsat}, which had advantage of avoiding under-sizing of the losses through imprecise features. The conduction losses in IGBT module were estimated as;

$$P_{tcond} = \frac{1}{T}\int_0^T V_{CEsat} i_t(t)dt \quad (6)$$

where T is electrical period of the sinusoid current i(t). For a bipolar sinusoidal modulation, the duty cycle was defined on basis that the modulating signal phase, modulation depth, and phase difference between the voltage and current of the load, followed modulating wave form,

$$e(t) = Msin(t) \quad (7)$$

where M is modulation rate, If the triangular carrier frequency f_p and the reference carrier frequency f_o were such that $f_o < f_p$, then the duty cycle could be put in the form,

$$\alpha(t) = \frac{\tau_h}{T_p} \approx \frac{1}{2}(1 + 2Msin(\omega t + \varphi) \quad (8)$$

where τ_h is period of time on (high output), T_p is period of triangular carrier, and φ is phase difference.

For a sinusoidal phase current, the conduction loss in the IGBT was expressed as,

$$P_{tcond} = \frac{1}{T}\int_0^T \alpha(t)V_{CEs0}I_{max}sin(\omega t - \varphi)dt + \frac{1}{T}\int_0^T \alpha(t)r_I I_{max}^2 sin^2(\omega t - \varphi)(t)dt \quad (9)$$

where φ is phase difference between the modulating signal image of the phase voltage V (as reference) and the current I of the same phase, r_I is internal resistance of IGBT, and V_{CEs0} is maximal drop voltage across the collector emitter terminals of IGBT in the on-state. Alternatively, the conduction losses in the IGBT could be expressed as,

$$P_{tcond} = \frac{V_{CEs0}I_{max}}{2}\left(\frac{1}{\pi} + \frac{M}{4}cos\varphi\right) + \frac{r_I I_{max}^2}{2}\left(\frac{1}{4} + \frac{2}{3}cos\varphi\right) \quad (10)$$

The conduction losses in the diodes were obtained by similar method as applied to the IGBT, but should be noted that a diode conducts only when the transistor which is in parallel is blocked. The two devices act complementary because if α(t) is the duty cycle of the transistor, then (1 – α(t)) is the factor for the diode. The diode conduction losses were expressed as,

$$P_{tcond} = \frac{V_{FO}I_{max}}{2}\left(\frac{1}{\pi} - \frac{M}{4}cos\varphi\right) + \frac{r_d I_{max}^2}{2}\left(\frac{1}{4} - \frac{2M}{3}cos\varphi\right) \quad (11)$$

where V_{FO} is forward voltage drop across the diode and r_d is internal resistance of the diode.

3.2.2. Switching losses in IGBT and diode

The switching losses were greater than conduction losses. A distinction was made between switching losses in the IGBTs and diodes. Switching losses in the blocking and priming of transistor were respectively expressed by,

$$P_{Toff} = t_{soff}I_{on}V_c f_{com} \quad (12)$$

$$P_{TOn} = t_{son}I_{on}V_c f_{com} \quad (13)$$

where V_c is continuous supply voltage, I_{on} is current status from the device, t_{son} is total switching time to boot, t_{soff} is total time of switching to the blocking, and f_{com} is switching frequency. Also the switching losses of diode are given by

$$P_{dcom} = \frac{E_{rr}I_{max}}{\pi I_{onoff}}f_{com} \quad (14)$$

where E_{rr} is dissipation energy accompanying diode extinction and I_{onoff} is manufacturer specified current.

3.2.3. Total losses in the inverter

The three-phase inverter had 6 power switches, and the total losses were,

$$P_{ond} = 6(P_D + P_T + P_{tr}) \quad (15)$$

where $P_D = P_{Dcom} + P_{Dcond}$ is total losses at a diode, $P_T = P_{Tcond} + P_{TOn} + P_{Toff}$ is total losses at a transistor, and P_{tr} are the parasitic losses of the chips determined as,

$$P_{tr} = \frac{1}{T}\int_{\varphi}^{\frac{T}{2}+\varphi} R_{CC'} - EE'I_{max}^2 sin^2(\omega t - \varphi)dt = R_{CC'} - EE'I_{max}^2/4 \quad (16)$$

where $R_{CC'} - EE'$ is conductive resistivity of semiconductor chips to the crossing of the current (values provided by Manufacturers).

3.3. Temperatures at Junctions

A thermal model was developed to determine the temperature rise at the semiconductor junctions of the electronic power modules.

The junction temperatures (°C) were expressed in terms of thermal resistances R (°C/W) and power P (W) by,

$$\Delta\theta_i = P_T\left(R_{j,bI} + R_{dbI}\right) + R_{d,a}(P_{tr} + P_T + P_T) \quad (17)$$

$$\Delta\theta_d = P_D\left(R_{j,bD} + R_{dbD}\right) + R_{d,a}(P_{tr} + P_T + P_T) \quad (18)$$

The thermal resistance of a layer was inversely proportional to the surface area, therefore, an increase of surface area led to decrease of thermal resistance; implying decrease of both average temperature and thermal ageing. For the same material thickness, an increase of surface area led to an increase of volume, and thereby influencing the mass and cost of the device. Hence, a compromise between average temperature and the total mass of the device must be achieved by optimized design.

4. ESTIMATION OF INVERTER MASS

The inverter mass was estimated on the assumptions that the chips were square in shape, mass of the metallization of the chips were negligible, total mass was three times that of the inverter arm, and the total mass of IGBT inverter was the sum of the masses of all the different components.

There are several types of hard solder depending on the type of alloy used [9, 10]. In the study, an alloy of SnAg with a respective proportion of 96.5 % and 3.5 % was chosen. The mass of hard solder of density ρ was determined as,

$$M_{br} = (0.965\rho_{sn} + 0.035\rho_{ag})(l_{br,i}L_{br,j} + l_{br,d}L_{br,d} + l_{cu}l_{sb})E_{br} \quad (19)$$

The semiconductors chips of IGBT and diode were made of silicon of density ρ_{si}, and was assumed that the semiconductor chips were square with thickness E_{dier}. Hence the masses were expressed as,

$$M_{IGBT} = \rho_{si}E_{die}c_i^2 \quad (20)$$

$$M_{diode} = \rho_{si}E_{die}c_d^2 \quad (21)$$

Copper layers covered the top and bottom surfaces of the substrate, and denoting the thickness by E_{cu}, width by l_{cu}, and length by l_{sb}, the mass formula was,

$$M_{cu} = 2\rho_{cu}E_{cu}l_{cu}l_{sb} \quad (22)$$

The substrate was aluminum nitride of thickness E_{sub}, and the mass estimated by assuming the same dimensions as copper was,

$$M_{sub} = \rho_{sub}E_{sub}l_{cu}l_{sb} \quad (23)$$

For providing mechanical support to the assembly of components, and effective heat transfer to a cold source, the sole was made of particle-reinforced silicon carbide aluminum plate of thickness E_{sole}, and the mass was expressed as,

$$M_{sem} = \rho_{sem}E_{sem}l_{sem}l_{sb} \quad (24)$$

The housing material was polybutylene terephthalate (PBT) plastic of thickness E_{boit} and height H_{boit}, and the mass was estimated assuming a rectangular shape by,

$$M_{boit} = \rho_{boit}E_{boit}(2H_{boit}(l_{sb} + L_{sem}) + l_{sb}L_{sem}) \quad (25)$$

The silicone gel provided enhancement of the electrical insulation, as well as protection of the semiconductor chips against humidity and oxidation, and also improved the resistance to partial discharges due to defects of DCB substrate metallization [11, 12]. Assuming that the gel filled all the empty space in the box after encapsulation, the mass was estimated as

$$M_{is} = \rho_{is}\left(l_{sb}L_{sem}H_{boit} - 2E_{puce}\left(c_i^2 + c_d^2\right) - E_{br}(2l_{br,i}L_{br,i} + 2l_{br,d}L_{br,d} + l_{sb}L_{sem}\right) - 2E_{cu}l_{cu}L_{sem} - E_{sub}l_{sb}L_{sem} \quad (26)$$

The heat sink was a radiator with a fin of base thickness E_{radiat}, and neglecting the mass of the fins relative to the base, the mass was,

$$M_{dis} = \rho_{dis}E_{radiat}l_{sb}L_{sem} \quad (27)$$

The total mass of the inverter was therefore determined by adding the masses of all the various components,

$$M_{ond} = 3(M_{sub} + M_{cu} + M_{isol} + M_{boit} + M_{sem} + M_{Diode} + M_{IGBT} + M_{solder} + M_{dis}) \quad (28)$$

5. LIFETIME PREDICTION

5.1. Lifetime Analysis

The lifetime of IGBT modules was predicted from the thermal ageing model, based on the temperature rise at the junctions IGBT housing and diode-housing. In general, the reference lifetime of insulation, τ_{ref} = 1.0 x 10^5 hr for a reference temperature of 40 ° C, but the lifespan is reduced to half value for each temperature rise of 10 ° C. Assuming a lifetime of 1.0 x 10^3 hr for temperature rise of 150 ° C, the corresponding model equation for lifetime prediction τ was given by the formula [13],

$$\tau = \tau_{ref}\ x\ 2^{[\Delta\theta_{avg}(a\Delta\theta_{avg}+b)]} \quad (29)$$

where θ_{avg} is average temperature of inverter; constant a = 3.979 x 10^{-4} $(°C)^{-2}$ and constant b = - 0.1040 $(°C)^{-1}$ were determined from the conditions that,

$\Delta\theta_{avg} = 10$ ℃; $\Rightarrow \tau = \frac{\tau_{ref}}{2} = 5.0\ x\ 10^4\ hr$ and $\Delta\theta_{avg} = 150$ ℃; $\Rightarrow \tau = 1.0\ x\ 10^3\ hr$.

The two antagonists fitness were the average temperature, $\Delta\theta_{avg}$ and the total mass of the device. Therefore, an optimization was necessary to find the best configuration based on the predicted lifetime. Increase of lifespan lead to decrease of heating temperature, and subsequent decrease in losses or mass increase. For a a balance between cost and lifetime, a multi-objective optimization was used by applying NSAG-II algorithm.

5.2. Optimization Process

The optimization was performed using Non-dominating Sorted Genetic Algorithm II (NSGA-II) [14, 15] and adapted Matlab Code (NGPM) [16]. The Matlab program was written for finite element optimization, but supported real and integer coding, and use genetic algorithm operators such as selection, mutation and crossover. For the selection, only binary tournament was supported.

The population used was a random initial population with uniform distribution number between the lower and upper bounds. The simulation was terminated when the maximum specified generation was reached. The Matlab program included an output function (.txt file); where the generated populations for all design variables, objectives and constraint violations (if exist) were found.

The interval between two calls of output function was an integer value, a parameter to be assigned. During the process, the populations were plotted and presented in GUI window step by step according to the specified value of corresponding parameter. The plot was the whole Pareto-optimal front with a well-distributed solution set in the front. Some of the optimization parameters are shown in Table 2.

Table 2. Optimization parameters

Parameter	Value
Population size	200
Maximum generation	500
Number of design variables	16
Number of objectives	2
Crossover operator	Intermediate, ratio=1.2
Mutation operator	Gaussian, scale=0.1, shrink=0.5

The two objective functions used for the optimization were the total mass of inverter and the average temperature of IGBT junction. The average temperature of IGBT was determined from the simplified thermal scheme of the inverter illustrated in Fig. 4. The total mass was determined from eqn. (28) taking into account the geometric model of the inverter, while the lifetime was calculated using eqn. (29).

The sixteen (16) variables used in the model calculations were c_d c_i L_{sem} $\ell_{br,i}$ $\ell_{br,d}$ ℓ_{cu} E_{br} E_{cu} E_{sub} E_{sem} E_{boi} H_{boi} E_{die} L_{sb} $L_{br,i}$ $L_{br,d}$, as listed in Table 3.

Table 3. Model variables

Geometrical parameters	Values (m)
c_d	$[10^{-3}, 6.0 \times 10^{-3}]$
c_i	$[2.0 \times 10^{-3}, 1.3 \times 10^{-2}]$
L_{sem}	$[10^{-1}, 3.6 \times 10^{-1}]$
$\ell_{br,i}$	$[3.05 \times 10^{-3}, 16.25 \times 10^{-3}]$
$\ell_{br,d}$	$[1.05 \times 10^{-3}, 6.25 \times 10^{-3}]$
ℓ_{cu}	$[2.5 \times 10^{-2}, 13 \times 10^{-2}]$
E_{br}	$[10^{-4}, 10^{-3}]$
E_{cu}	$[1.5 \times 10^{-4}, 3.0 \times 10^{-4}]$
E_{sub}	$[10^{-3}, 6.3 \times 10^{-3}]$
E_{sem}	$[10^{-5}, 2.0 \times 10^{-3}]$
E_{boi}	$[10^{-3}, 5.0 \times 10^{-3}]$
H_{boi}	$[3.2 \times 10^{-2}, 4.0 \times 10^{-2}]$
E_{die}	$[1.5 \times 10^{-4}, 3.5 \times 10^{-4}]$
L_{sb}	$[2.0 \times 10^{-2}, 9.0 \times 10^{-2}]$
$L_{br,i}$	$[1.5.0 \times 10^{-2}, 7.0 \times 10^{-2}]$
$L_{br,d}$	$[10^{-2}, 5.0 \times 10^{-2}]$

5.3. Pseudo-Code for NSAG-II and Matlab Program

The population P_o was initialized using uniform distribution of random number between the lower and upper bounds. Once P_o was created, a sort of population based on non-dominance solution was performed. Each solution was assigned a rank corresponding to level of dominance; 2 (best), 2 (better), and so on; thus minimization of fitness was assumed. Using binary tournament selection, recombination and mutation operators, a new population Q_o was created at end of the first, of the same size N than latter. Combining the two populations, a new population of size N was obtained, sorted out based on non-dominance and crowding distance solutions.

On obtaining several fronts, simulation moved onto the next generation P_1 choosing solutions from the first non-denominated one; and

if the size was not reached, moved on to the next edge solution, and so on, until new generation P_1 of size N was obtained.

The process was repeated until maximum number of generation level was reached. Diversity of non-dominated solutions was introduced using the procedure of space comparison, which was used in the selection of the tournament during the reduction of population.

The steps for the pseudo-code were:

- Create initial random population of size N;
- Evaluate lifetime τ and total mass (M);
- Use binary tournaments selection, recombination and mutation operators to create offspring population of N;
- Sort combined parent and offspring population (size 2N) into Pareto-ranks using fast non-dominated sorting;
- Create new generation population by selecting from N population members;
- Repeat step 3.

The listed main Matlab program of NSGA-II were:

```
clc; clear; close all
options = nsgaopt_ondul(); % create default
          options structure
options.popsize = 200;     % population size
options.maxGen = 500;      % max generation
options.numObj = 2         % number of objectives
options.numVar = 16;       % number of design
                  variables
options.numCons = 3;       % number of constraints
option.nOvervar = 0;       % number of over
                  variables completed
options.lb = [];           % lowers bounds of variables
options.ub = [];           % upper bounds of variables
options.objfun = @Inverter_objective; % objective
                  function handle
options.plotInterval = 10;      % interval between
                  two calls of "plotnsga".
result = nsga2_ondul(options);       % begin the
                                     optimization!
```

6. RESULTS

After the optimization process, Pareto-optimal front of the two fitness presented all the possible configurations of the inverter as shown in Fig. 5. Hence, the predicted lifetime versus the mass is presented in Fig. 6.

When the mass was increased, the average temperature decreased, such that the copper losses reduced and the inverter efficiency increased. The increase of the mass meant an increase in the cost of the inverter. For each point in a made according to the system lifetime. Consid-

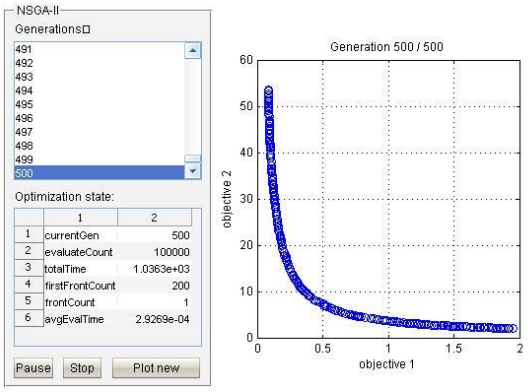

Fig. 5. Pareto optimal front of average temperature and mass

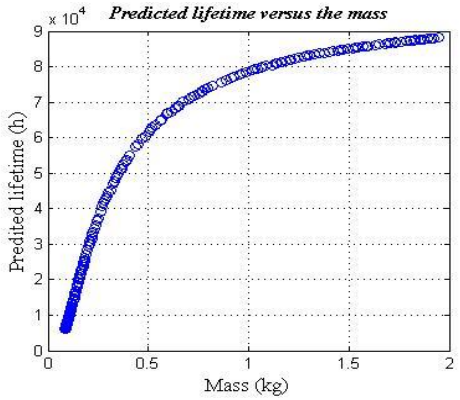

Fig. 6. Predicted lifetime versus the mass

ering a PV system, there are several possible choices taking into account the panel lifetime and the daily operation.

For example, with a panel of lifetime of about 25 years, under daily operation time of ~ 8 hrs, the system would work for 72,000 hrs. Therefore, the lifetime of the inverter could be predicted as shown in Fig. 7(a). For both geometric and thermal ageing models, no configuration corresponded to the duration and the nearest was chosen.

For the predicted lifetime equivalent to mid-lifetime of the panel, the system would work for 36,000 hours, and the corresponding life-time and mass of inverter are presented on the Fig. 7 (b).

7. DISCUSSION

Two objective functions used for the simulations were the total mass determined from geometric model of the inverter, and average temperature of IGBT determined form thermal ageing model. The two approaches of optimal design were demonstrated by the evolution

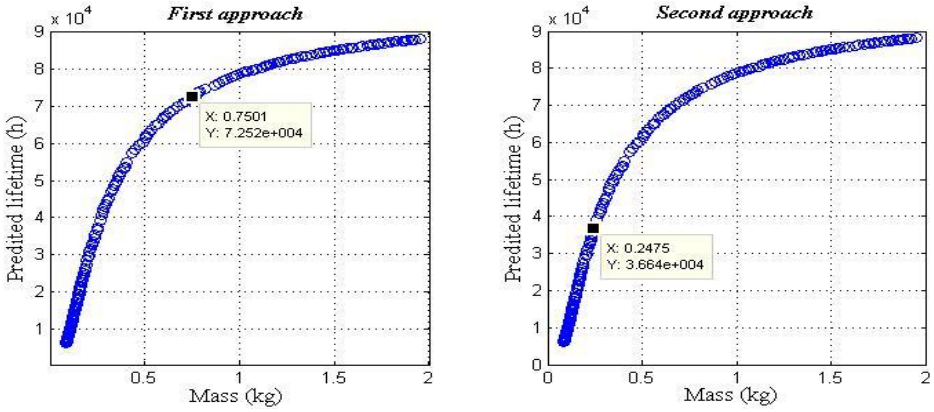

(a). (b).

Fig.7. Two examples of approach (a) 72,000 hrs, (b) 36,000 hrs

of average temperature and lifetime of IGBT as the total mass of the inverter increased.

The increase of inverter mass meant additional cost, and a better economic solution would be to select an inverter of lifetime equal to half of lifetime of the solar panel. A change of inverter mass from 1 kg to about 0.3 kg is most feasible and efficient, and replacement of inverter after half of the lifespan of the panels is recommended.

8. CONCLUSIONS

Geometrical configuration, thermal ageing and total mass calculations were considered for multi-criteria optimization using NSAG-II algorithm to predict the lifetime of IGBT inverter. For the optimal design, a compromise between mass and heating was analysed to optimize and control the operational cost and selection of a more robust system.

For better sustainability of grid connectivity of systems with solar inverters, a replacement of the inverter after half of the lifespan of the panels is reasonable. The suggestion is plausible even if the investment related to replacement seems high initially, because the reduction of the duration of the inverter lifetime allows a significant reduction in the mass of the device.

9. REFERENCES

1. Ciappa M., Selected failure mechanisms of modern power modules, *Microelectronics Reliability*, 42, 2002, pp. 653–667.
2. Smet V. and Forest F., Ageing and failure modes of IGBT Modules in high-temperature power cycling, *IEEE Transactions no Industrial Electronics*, Vol. 58, No. 10, 2011.
3. INFINEON, Dimensioning program IPOSIM for loss and thermal calculation of Infineon IGBT modules, *Technical Documentation*, 2006, p. 20.
4. Agbokpanzo R.G. and Houngan T.K., Etude du comportement dynamique d'un système de pompage photovoltaïque dans Matlab/Simulink, *J.R. Sci. Univ. Lomé (Togo)*, Série E, 16 (1), 2014, pp: 129 - 138.
5. Hsieh C.Y. and Chung S.L., High thermal conductivity epoxy molding compound filled with a combustion synthesized AIN powder, *J. Applied Polymer Sci*., Vol. 102, No. 5, 2006, pp. 4734 - 4740.
6. Jiao J., Cui Y. and Yu Xia Y., Improved thermal conductivity of epoxy composites prepared with a mixed filler of multiwalled carbon nanotubes and aluminum nitride particles, *SAGE J. High Performance Polymers*, 2016.
7. Turbini L.J., Processing and material issues related to lead-free soldering, *J. Mater. Sci. Mater El ectron*, Vol. 18, 2007, pp. 147–154 (DOI 10.1007 /s10854-006-9014-6).
8. Occhionero M.A., Hay R.A., Adams R.W. and Fennessy K.P., Aluminum Silicon Carbide Thermal management packaging for high density packaging applications, in *Proc. Ceramics Process Systems Corp*., Chartley, Denver, CO., April 6 - 9, 1999, http://www.alsic.com.
9. Fenner M., Understanding the impact of pb-free on solder paste, *EPP Europe Magazine*, 2003.
10. Schleuning D., Griffin M., James P., McNulty J., Mendoza D., Morales J., Nabors D., Peters M., Zhou H. and Reed M., Robust hard-solder packaging of conduction cooled laser diode bars, in *Proc. SPIE High-Power Diode Laser Technology and Applications*, 2007, SPIE 6456, Vol 645604.
11. Wang N. and Cotton I., Impact of thermal cycling in humid environments on power electronic modules, *IEEE Transactions on Components, Packaging and Manufacturing Technology*, Vol. 2, No. 7, 2012, pp. 1085 – 1091.
12. Lebey T., Malec D., Bleyl V., Breit F. and

Dutarde E., Contribution to the dimensioning of the different insulating materials used in high voltage power electronics module manufacturing, in *Proc. 5th Intern. Conf. on Power Electronics and Drive Systems*, PEDS 2003, Vol. 1, IEEE.
13. Bonnett A.H., Cause and analysis of stator failures in three-phase squirrel-cage induction motors, *IEEE Transactions on Industry Applications*, 1992, pp. 921 - 837.
14. Deb K., Pratap A., Agarwal S. and Meyarivan T., A fast and elitist multiobjective genetic algorithm: NSGA-II, *IEEE Transactions on Evolutioonary Computation*, 2002, pp. 182 – 197.
15. Deb K., Multi-Objective optimization using evolutionary algorithms, An Introduction., Indian Institute of Technology Kanpur, *KanGAL Report*, 2011, p. 24.
16. Song L., *NGPM - NSGA-II Program in Matlab*, College of Astronautics, 2011, Northwestern Polytechnic University, China.